An Experimental-Numerical Study of Heat Transfer Enhancement in a Minichannel Using Asymmetric Pulsating Flows

Parth S. Kumavat, Sajad Alimohammadi, and Séamus M. O'Shaughnessy

***Abstract*— The development of current and next-generation high-performance electronic devices has led to miniaturization in more densely packed spaces. The increasing power levels have resulted in ever-increasing heat flux densities which necessitates the evolution of new liquid-based heat exchange technologies. Implementation of single-phase cooling systems using pulsating flow is viewed as a potential solution to the problems involving high energy density electronics. This work involves a combined experimental and numerical analysis of pulsating flows in a rectangular minichannel undergoing asymmetric sinusoidal flow pulsation formats. The minichannel design includes a heated bottom section approximated as a constant heat flux boundary by uniformly heating a 12.5 μm thick Inconel foil. Infrared thermography (IRT) is used for thermal measurements of the heated boundary from the hydrodynamically and thermally developed region of the minichannel. A 3-D conjugate heat transfer ANSYS CFX model is used for simulations. Asymmetric sinusoidal pulsating flows in the form of leading and lagging profiles with Womersley number of 2.5 and a flow rate amplitude ratio of 0.5 and 3 are investigated. The rapid fluctuating characteristics of the asymmetric waveforms cause a sudden shift in the flow velocity profiles and the subsequent increased pressure drop shows an evolution of phase lag. The intensification of fluid momentum due to high oscillating flowrate amplitudes causes enhanced mixing in the near-wall and bulk regions of the channel, as evidenced by the wall temperature profiles. The presence of wall viscous forces leads to the phenomenon of annular effects which has been widely investigated in the literature for symmetric flow profiles. The wall and bulk temperature profiles tend to readily adjust to this rapidly fluctuating flow. The effect of high pulsation flow rate amplitude leads to a heat transfer enhancement of about 11% over the corresponding steady flow.**

***Index Terms*— Conjugate heat transfer, flow rate modulation, heat transfer enhancement, oscillating flow, pulsating flow.**

Manuscript received 15 April 2023; revised 3 July 2023; accepted 6 July 2023. Date of publication 26 July 2023; date of current version 20 September 2023. This work was supported in part by the School of Engineering, Trinity College Dublin under Award 1272. Recommended for publication by Associate Editor L. Codecasa upon evaluation of reviewers' comments. *(Corresponding author: Parth S. Kumavat.)*

Parth S. Kumavat and Séamus M. O'Shaughnessy are with the Department of Mechanical, Manufacturing and Biomedical Engineering, Trinity College, University of Dublin, Dublin, D02 PN40 Ireland (e-mail: kumavatp@tcd.ie; oshaugse@tcd.ie).

Sajad Alimohammadi is with the School of Mechanical and Design Engineering, Technological University Dublin, Dublin, D07 EWV4 Ireland (e-mail: sajad.alimohammadi@tudublin.ie).

Color versions of one or more figures in this article are available at https://doi.org/10.1109/TCPMT.2023.3299085.

Digital Object Identifier 10.1109/TCPMT.2023.3299085

I. Introduction

LIQUID cooling systems are a potential approach to meet the challenge of futuristic, miniaturized, and high-energy density circuits and photonics. Unsteady pulsating flows are employed in a range of industrial applications owing to their characteristic near-wall fluctuating velocities, leading to enhanced heat dissipation. Applications of pulsating flows include heat exchangers, pulse-tube cryocoolers, and cooling of electronics, e.g., thermoelectric module cooling for battery thermal management systems [1], micro-fluidic dual piezoelectric pulsed jet cooling [2], rack-component enclosure cooling [3], [4], [5], and microchannel manifold heat sinks [5]. A pulsating flow [Fig. 1(b)] is a non-zero mean mass flow which comprises an oscillating or zero mean mass flow [Fig. 1(a)] superimposed on a steady flow. The waveform amplitude and frequency (f) link the viscous-inertial characteristics of pulsating flows to the local, transient heat transfer. The phase angle $\theta = \omega t$ describes the periodic progression of the waveform.

Several dimensionless numbers are used to describe pulsating flows. For the flow of a fluid with a velocity V and kinematic viscosity ν through a duct of hydraulic diameter D_h, the Reynolds number, defined as $\mathrm{Re} = VD_h/\nu$, represents the ratio of inertial and viscous time scales. The Womersley number, $Wo = (D_h/2)(\omega/\nu)^{1/2}$, quantifies the ratio of oscillating and diffusive time scales, where $\omega = 2\pi f$ is the oscillating angular velocity [6]. For a pipe/channel flow, a variation in Wo alters the velocity profiles, e.g., parabolic for viscous dominated flows ($Wo \ll 1$), more uniform or flatter velocity profiles for $Wo \approx 1$, and distinct near-wall velocity peaks for inertia dominated flows ($Wo \gg 1$). The flow rate amplitude is defined as $A_0 = Q_{\text{osc.max.}}/Q_s$ and represents the ratio of the maximum oscillating flow rate ($Q_{\text{osc.max.}}$) to the steady flow rate (Q_s). A_0 can also influence the flow behavior and heat transfer through flow reversal effects which typically occur at values $A_0 > 1$.

Pulsating flows are an active research area and several studies have indicated the potential for appreciable heat transfer enhancement. Recent studies by [7] using square flowrate profiles in a uniformly heated minichannel with $0.8 \leq Wo \leq 5.9$ and $A_0 = 0.92$ indicated a marginal enhancement for higher frequencies. Zhang et al. [5] indicated heat transfer enhancement of up to 17% for larger flowrate amplitude ($0.01 \leq A_0 \leq 5$) with sinusoidal flow pulsations for a slotted microchannel heat sink when using non-Newtonian fluids. Walsh et al. [8] have utilized an oscillatory flow device to

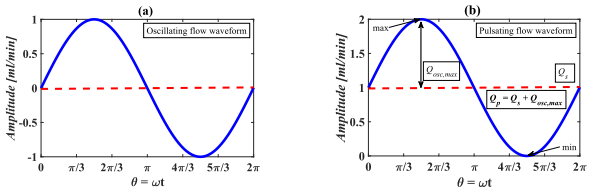

Fig. 1. Examples of oscillating and pulsating flow waveforms.

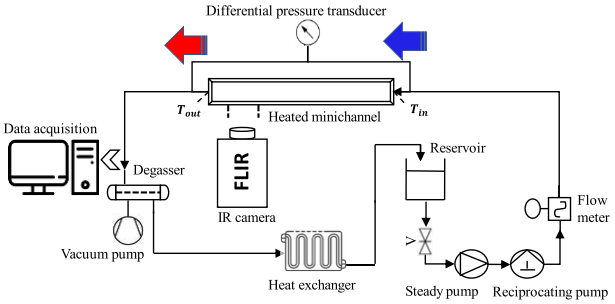

Fig. 2. Schematic of the experimental setup.

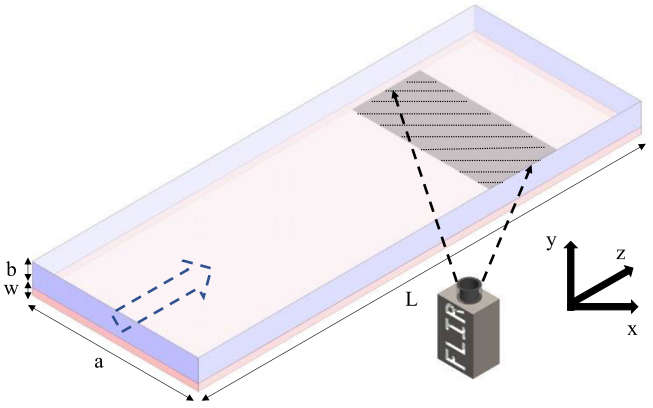

Fig. 3. Minichannel cross section with the heated foil.

reduce operating temperatures in a microelectronic PC cabinet by as much as 40% compared with steady flow temperatures. Wälchli et al. [9] implemented a hybrid cooling system consisting of a microchannel heat absorber and heat dissipator to facilitate efficient heat removal. A reciprocating water flow loop was used. In their subsequent study, Wälchli et al. [10] found that a peak cooling performance of 180 W/cm^2 was achieved with moderately high frequencies using a pumping power of only 1 W. A time-dependent analytical analysis of bulk fluid temperature carried out by [11] predicted a reduction in heat transfer for the first half-cycle and an enhancement in heat transfer for the second half-cycle of a sinusoidal flow pulsation for $1.4 \leq Wo \leq 22.1$.

Xu et al. [12] used square, sawtooth, triangular, and sinusoidal excitation waveforms for nanofluid flow through microchannel heat sinks for frequencies $1 \leq f \leq 4.5$, showing insignificant heat transfer for all waveforms except square. With a considerable increase in pumping power and high flow frequency, the nanofluids indicated an enhancement in heat transfer of about 3.1% over pure water for a square waveform. In another microchannel study by [13] which employed particle image velocimetry (PIV), the effects of asymmetric triangular and sinusoidal flow pulsations were studied for a Womersley number range $1 \leq Wo \leq 5$. Results showed a heat transfer reduction for conventional pulsatile waveforms due to inefficient narrowing of the thermal boundary layer. Contrastingly, the asymmetric flows showed intense fluid mixing with a rapid shift in flow velocity and corresponding pressure gradients, leading to an enhancement of up to 28% over steady flow.

Investigations of heat transfer relating to asymmetric pulsating flow waveforms are underrepresented in the literature. This study follows the work of Blythman et al. [14] and is an extension of work presented at THERMINIC 2022 [15] and concerns pulsating flow in a heated rectangular minichannel, which is experimentally and computationally investigated for leading and lagging asymmetric sinusoidal waveforms of pulsation frequency $f = 0.5$ Hz, corresponding to $Wo = 2.59$ where unconventional velocity profiles with near wall peaks are anticipated. In addition, flow rate amplitudes of $A_0 = 0.5$ and 3 are investigated to discover the effects of flow reversal on the wall heat transfer. New data from simulations performed using ANSYS CFX are provided, and these data are validated by experiments performed using infrared thermography (IRT) techniques. The overarching aim is to exploit the characteristics of pulsating flow for efficient heat removal without compromising net mass transport.

II. Experimental Methodology

The experimental setup is an ordered assembly of multiple plates clamped rigidly together, as shown by the schematic in Fig. 2. At the base section is the heater support plate, made from Ertacetal material, which houses two pairs of copper electrodes also known as busbars. The copper busbars extend along the axial (z) direction of the rig and function to supply up to 42 A of current to a laterally tensioned Inconel 600 foil of 12.5 μm thickness. Inconel was selected for its low thermal conductivity, limiting lateral conduction effects, and high resistivity that results in higher heat fluxes at lower supply currents. The foil approximates a constant heat flux boundary condition and forms the bottom surface of the minichannel. Foil tensioning is achieved using a spring-loaded bolt system which pulls the foil through the busbars pairs. A machined rectangular minichannel of length $L = 360$ mm, width $a = 20$ mm, and height $b = 1.4$ mm is placed on top of the foil of thickness $w = 12.5$ μm. The channel hydraulic diameter $D_h = 2.62$ mm. The minichannel aspect ratio (AR) is 14.2. Based on an analytical study of wall temperature distributions in rectangular ducts by [16], the effect of peripheral heat conduction as a function of fluid conductivity, AR, and imposed heat flux was established. The optimum AR was determined to be in the range of $10 \leq AR \leq 20$ wherein large reductions in peak fluid temperatures were observed compared to smaller ($AR < 10$) and larger ($AR > 20$) AR channels, since the heat concentrations were found to occur at corner regions. A 1 mm ID rubber O-ring is fit at the foil and channel interface to prevent leakages. The minichannel, with one heated long wall and all other walls insulated, approximates the experimental configuration identified as H2(1L) [10], [11], [12], [13]. A sketch of the minichannel cross section is shown in Fig. 3.

Equation (1) calculates the uniform electrical heat generation in the foil by Joule heating. De-ionized water is supplied to the channel in a closed flow loop connecting the inlet and outlet. Heat removed from the foil is subsequently removed

from the water by a fan-driven plate-fin heat exchanger before returning to the channel inlet. The fluid is initially degassed through a hollow fiber membrane module by a vacuum pump. The experimental configuration ensures a hydrodynamically and thermally developed flow in the minichannel test section where the IR measurements are recorded. The estimation of hydrodynamic entrance length (L_e) is given by [20], shown here in (2). The maximum Reynolds number $\mathrm{Re}_{\max} = \mathrm{Re}_s + \mathrm{Re}_{\mathrm{osc.max}} = 205$, predicts a laminar flow with an equivalent pulsating flow hydrodynamic entry length of $L_e = 23.94$ mm. For reference, the entry length for pulsating pipe flow has been shown numerically to vary sinusoidally with an amplitude less than or equal to the steady flow value [21]. The channel entry length for thermally developed flow is calculated by $\mathrm{Pr} \times L_e = 167.58$ mm. Hence, a 220 mm heated length upstream of the IR viewing window ensures developed flow

$$q_{\mathrm{gen}} = \frac{I^2 R}{L_f a_f} \tag{1}$$

$$\frac{L_e}{D_h} = \left[(0.631)^{1.6} + (0.0442\mathrm{Re}_s)^{1.6}\right]^{\frac{1}{1.6}}. \tag{2}$$

During the experiments, the flow is driven by a McLennan 34HSX-108 stepper motor controlled by an ST5-Q-NN Applied motion drive, which offers precise control over the pulse generation resolution with a range of 25 000 steps per revolution, with frequencies up to 25 Hz. A National Instruments NI-DAQ 9269 is used in conjunction with LabVIEW to modulate the frequency and amplitude of the function generator. An Atrato 710 series noninvasive ultrasonic flowmeter is attached close to the inlet section of the flow to record precise flow rates. A high accuracy calibrated differential pressure transducer measuring pressure differences up to 17.24 kPa (OMEGA PX 409 series) is connected between the inlet and outlet sections of the minichannel, 10 and 180 mm downstream of the inlet.

This study focuses on the experimental investigation of unsteady asymmetric sinusoidal flows defined by a special case of the Clausen function integral (Cl_2) [22]. The waveform phase is defined by θ in the range $0 \le \theta \le 360°$, and t is the period of the waveform. Leading (−ve) and lagging (+ve) asymmetric profiles are obtained from (3), which must be multiplied by the flow rate amplitude to obtain the oscillating flow rate

$$\mathrm{Cl}_2(\theta) = \pm \int_0^{\theta} \ln\left[2\sin\left(\frac{1}{2}t\right)\right] dt. \tag{3}$$

Four calibrated type-T thermocouples record temperatures at the inlet and outlet of the minichannel and the air temperature in the cavity between a sheet of IR transmitting glass and the underside of the heated foil. Only a small section of the underside of the foil is visible and this section is carefully coated in high-temperature matte black to increase the surface emissivity to 0.95 and to prevent reflections. A 1 mm thick sapphire glass window is placed approximately 13.5 mm beneath the painted foil to enclose the region and limit heat loss. This glass is transparent to infrared (IR) radiation. The glass forms a cavity, heated from above, in which the heat transfer mode can be approximated as 1-D conduction, as described by [23]. The foil temperatures are recorded

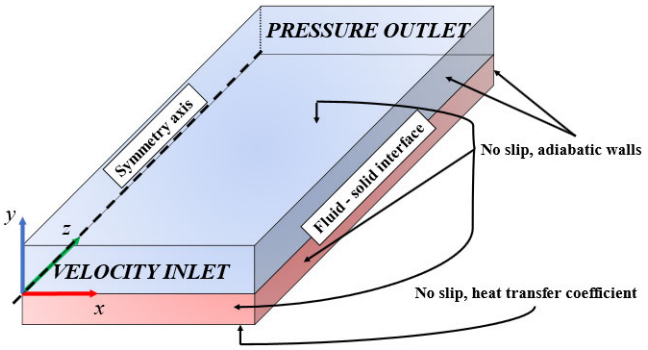

Fig. 4. Three-dimensional computational domain and boundary conditions. Blue and red regions are fluid and solid domains, respectively.

non-intrusively using a FLIR SC6000 high-speed, high-resolution, and infrared camera. This camera has a maximum 640 × 512-pixel focal plane array, sensitivity in 2.5–5.1 μm range, and is used to obtain time-resolved and space-resolved wall temperature measurements. Prior to the testing, a two-point non-uniformity correction (NUC) is performed with a blackbody calibrator, and an in situ calibration is performed, as researched by [24]. The camera reads an external TTL pulse trigger signal from the motor control to facilitate phase-lock measurements to the flow oscillations. The video files are processed in MATLAB.

To evaluate the thermal performance of heated minichannels under pulsating inlet conditions, convective heat transfer parameters are introduced. For the equations presented below, time averaging is performed over one pulsation cycle (λ) once the periodic behavior is established. Spatial averaging is performed over the range 0 mm $\le x \le$ 20 mm. All measurements are recorded at $z \ge 220$ mm, i.e., where the flow is expected to be fully developed hydrodynamically and thermally. $\overline{T_w}$, as defined by (4), is the time-averaged heated wall temperature. $|T_w|$ is the instantaneous spatially averaged temperature along the heated wall. $\overline{T_b}$ is the time-averaged bulk fluid temperature as given by (5). T_{in} and T_{out} are instantaneous fluid temperatures determined from the inlet and outlet thermocouples. The time-space averaged Nusselt Number ($|\overline{\mathrm{Nu}}|$) as given by (6) defines the relationship between the fluid thermal conductivity (k_l) and surface convection. The overall uncertainty of $|\overline{\mathrm{Nu}}|$ is about 6%, owing to the higher uncertainties for wall and bulk temperatures. The time-space averaged foil heat flux is defined as ($|\overline{q}_w|$). The normalized enhancement of heat transfer compared to steady flow only is described by (7) where Nu_s represents the steady flow Nusselt number. To characterize the performance of the asymmetric sinusoidal flow pulsations in terms of heat transfer and pressure drop, a thermal performance parameter η is defined as given by (8). The time averaged friction factor for pulsating flow ($\overline{\sigma}_p$) is obtained from Darcy–Weisbach equation, described by (9) where (ΔP) is the pressure drop. σ_s is the corresponding friction factor for steady flow at the same Reynolds number (Re). For a steady flow with average velocity U_s, $\eta = 1$. For pulsating flows, $\eta < 1$ signifies a reduction of the thermal-hydraulic performance compared to steady flow, and $\eta > 1$ signifies an improvement

$$\overline{T}_w = \frac{1}{\lambda}\int_0^{\lambda} |T_w| dt \tag{4}$$

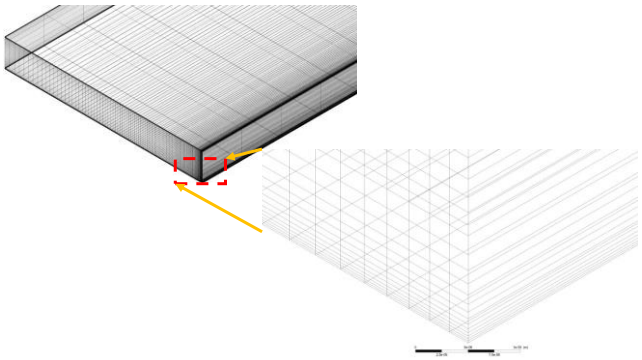

Fig. 5. Two-staged 3-D isometric view of the mesh, inclusive of solid and fluid domains.

$$\overline{T_b} = \frac{1}{\lambda}\int_0^{\lambda} \frac{(T_{\text{in}} + T_{\text{out}})}{2} dt \tag{5}$$

$$|\overline{\text{Nu}}| = \frac{|\overline{q}_w| \cdot D_h}{\left(\overline{T_w} - \overline{T_b}\right) \cdot k_l} \tag{6}$$

$$d\text{Nu} = \frac{|\overline{\text{Nu}}| - \text{Nu}_s}{\text{Nu}_s} \tag{7}$$

$$\eta = \left(\frac{\overline{\text{Nu}}_p}{\text{Nu}_s}\right)\left(\frac{\overline{\sigma}_p}{\sigma_s}\right)^{-1/3} \tag{8}$$

$$\overline{\sigma}_p = \frac{1}{\lambda}\int_0^{\lambda} \frac{2(\Delta P/L)D_h}{\rho U_s^2} dt. \tag{9}$$

III. Numerical Methodology

A 3-D conjugate heat transfer computational model is developed which approximates the experimental conditions. The geometry consists of a cuboidal fluid domain of length $L = 360$ mm, width $a = 10$ mm, and height $b = 1.4$ mm on top of a solid domain of equal length and width but thickness $w = 12.5$ μm. Water, with a density of 1000 kg/m^3, the dynamic viscosity of 8×10^{-4} Pa·s, specific heat capacity of 4137 (J/kg)·K, and thermal conductivity of 0.6 W/m·K, is specified as the working fluid. The solid domain material is defined as Inconel 600 with a density of 8420 kg/m^3, the specific heat capacity of 444 (J/kg)·K, and thermal conductivity of 14.9 W/m·K. A volumetric heat source of 3.6×10^8 W/m^3 is applied to the solid for all simulations. A laminar viscous model is adopted for steady and transient computations. A finely resolved structured grid is used for both fluid and solid domains. Refinement in the form of inflation layers is provided toward the minichannel boundaries to capture the steep velocity and thermal gradients near the walls. The computational domain as illustrated in Fig. 4 shows the imposed boundary conditions. A uniform temperature and velocity inlet boundary condition is defined. A user-defined function (UDF) simulates the leading and lagging asymmetric sinusoidal pulsations. A zero gradient pressure outlet boundary condition is imposed at the exit of the minichannel with 0 Pa as the gauge pressure. The model is set with an operating pressure of 101 325 Pa. Further, the top and side walls are approximated with no-slip and adiabatic conditions for the fluid and solid domains, respectively. Whereas the bottom wall of the solid domain is defined with a heat transfer coefficient accounting for the approximated experimental heat loss from the underside of heated foil.

To reduce the computational requirements, a symmetry condition is imposed on one long face of the minichannel which assumes zero flux of all quantities across it. The *General Grid Interface* technique is the default method for conjugate heat transfer problems in ANSYS CFX and permits an adaptable mesh connection of the non-conformal, non-matched grids across the solid-fluid interface. Following mesh verification studies using coarse, medium, and fine grids, the generated (fine) grid, shown in Fig. 5, consists of 1 718 669 structured hexahedral cells, refined at the entry and wall boundaries to capture the near wall gradients. Considerations were given to mesh quality, skewness, AR, etc. ANSYS CFX is a coupled solver which follows a vertex-centered approach wherein the solution variables are stored in the mesh vertices (nodes). Adaptive time stepping is used to maintain low Courant Friedrichs-Lewy numbers (CFL $<$ 5). A second-order upwind spatial discretization scheme is chosen for the convective terms of momentum and energy equations. Diffusion terms are calculated based on element shape functions and are second-order accurate. The pressure term is corrected by applying a fourth-order correction term which prevents pressure-velocity decoupling. A high-resolution advection scheme is preferred since it optimizes between the first and second-order differentiation to maintain the solution boundedness to achieve higher accuracy of convergence. A rms scaled residual value of $<10^{-5}$ is used as convergence criteria for governing equations. Parameters such as bottom wall temperature, mass flow inlet, and outlet are used to assess convergence which typically occurs after 20 cycles of pulsation.

Mesh verification and model validation studies were previously carried out by the authors for cases employing symmetric sinusoidal waveforms. Details, including a comparison with published literature, are provided in [19]. Following a similar procedure, the calculated grid convergence index (GCI) for this study is 1.2%.

IV. Results and Discussions

The following figures present a results comparison between experiments and CFD simulations. Overall, there is a reasonable overall agreement between the experimental and numerical results. Greater discrepancies exist in the cases of higher flow rate amplitude due to the experimental measurements where very sudden high-pressure gradients are introduced to the minichannel by asymmetric flow pulsations. Minor differences exist between the experimental and numerical temperature data due to the existence of small magnitudes of temperatures in the oscillating and steady cases which can be of the order of the IR camera sensitivity. Fig. 6(a)–(d) presents the temporal variation of normalized oscillating volumetric flow rate (Q_{osc}/Q_s), normalized pressure gradient ($\nabla p_{\text{osc}}/\nabla p_s$), and normalized wall shear stress (τ_{osc}/τ_s) in response to a leading and lagging asymmetric pulsation waveform for a frequency of $f = 0.5$ Hz ($Wo = 2.5$) at flow rates amplitudes $A_0 = 0.5$ and 3. Oscillating parameter values represent pulsating flow values minus the steady flow values. The oscillating parameters in Fig. 6 are normalized by their corresponding steady flow value. The leading asymmetric waveform as shown in Fig. 6(a) and (b) exhibits an initial period of rapid acceleration followed by a gradual deceleration before another

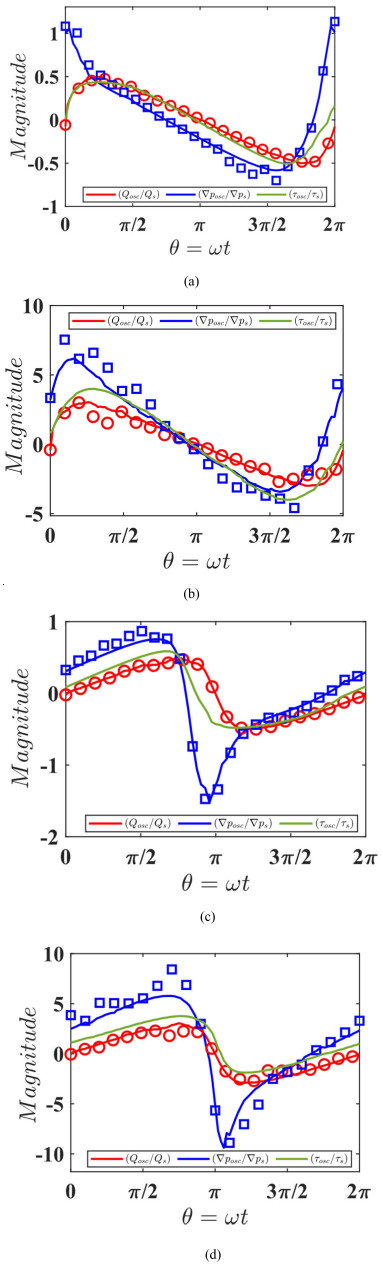

Fig. 6. Temporal variation of the normalized oscillating flowrate, normalized oscillating axial pressure gradient, and normalized oscillating bottom wall shear stress. Solid lines represent CFD data, markers show the experimental data. (a) Leading asymmetric sinusoidal waveform, $f = 0.5$ Hz, $Wo = 2.5$, $A_0 = 0.5$. (b) Leading asymmetric sinusoidal waveform, $f = 0.5$ Hz, $Wo = 2.5$, $A_0 = 3$. (c) Lagging asymmetric sinusoidal waveform, $f = 0.5$ Hz, $Wo = 2.5$, $A_0 = 0.5$. (d) Lagging asymmetric sinusoidal waveform, $f = 0.5$ Hz, $Wo = 2.5$, $A_0 = 3$.

cycle of rapid acceleration phase with the restart of the cycle. The fluctuations induced by the asymmetric flows lead to a substantial increase in the pressure gradient as is seen for the high flowrate amplitude cases of Fig. 6(b) and (d) compared to symmetric sinusoidal flows described in [12] and [13]. Similarly, [13] observed that asymmetric flows generated a sharp impulse of flow momentum which leads to a significant amplification of pressure oscillations with an overall increased pressure drop in the channel. There exists a maximum phase lag of 41° between the pressure gradient and the other profiles, as seen in Fig. 6(a). With the increase in flow rate amplitude to $A_0 = 3$, there is a simultaneous increase in the pressure amplitude with very high values observed during the onset of the accelerations at the start and end of the pulsation. However, a minimal effect is observed for the bottom wall shear stress with a small phase lag of 5° as observed in Fig. 6(a). Whereas with an increase in flowrate amplitude, the magnitude of shear stress increases as seen in Fig. 6(b) since the maximum fluid velocity increases sharply.

The lagging asymmetric waveform features an initial period of gradual acceleration followed by a shortened acute impulse in the deceleration stage with another gradual acceleration stage to complete the cycle, as shown by Fig. 6(c) and (d). Due to the rapid alterations in the fluid momentum over a short time interval, a sharp impulse in the pressure gradient is seen in Fig. 6(d) at phase interval π for the higher flowrate amplitudes $A_0 = 3$. Similar to the characteristics observed in the case of the leading asymmetric profile, Fig. 6(c) presents a phase lag between the pressure gradient and flowrate profiles with a phase lag of 29°. In the case of wall shear stress, a less prominent phase lag is developed compared to the pressure gradient profiles. However, at $A_0 = 3$ [see Fig. 6(d)], the resulting shear stress is increased in response to the enhanced bulk flow fluctuations.

Fig. 7(a)–(d) shows the spanwise variation of the corresponding phase-averaged oscillating heated wall temperature profiles ($\overline{T_{w,\mathrm{osc}}}$) from the fully developed region of the channel at $z = 0.3$ m. Lines and markers represent CFD and experimental data, respectively, shown as a function of the non-dimensional minichannel width (x/a) along the heated wall (i.e., at $y/b = 0$). Fig. 7(a)–(d) plots data for leading and lagging asymmetric sinusoidal waveforms, respectively. The widely established phenomenon of annular effect for pulsating flows, as reported by authors in [13] and [19] for experimental and numerical studies involving symmetric sinusoidal flow profiles, is also evident in the oscillating wall temperature profiles of leading and lagging asymmetric sinusoidal waveforms at both $A_0 = 0.5$ and 3. This is a result of high near-wall velocity fluctuations, indicating enhanced heat dissipation from near-wall regions to bulk. On increasing A_0, steeper thermal gradients are obtained in the near side-wall vicinity $0.8 \leq x/a \leq 1$ as the effect of the more pronounced acceleration stage during phases $0 \leq \theta \leq \pi/2$ and $3\pi/2 \leq \theta \leq 2\pi$ seen previously in Fig. 6. An increase in the flow rate amplitude leads to stronger forced convection, leading to a drop in wall and bulk temperatures.

Fig. 8(a)–(d) plots the temporal variation of the oscillating wall ($T_{w,\mathrm{osc}}$) and oscillating bulk temperature ($T_{b,\mathrm{osc}}$) profiles as well as the difference between the two ($T_{w,\mathrm{osc}} - T_{b,\mathrm{osc}}$) for leading and lagging asymmetric waveforms. The figures present a clear influence of the waveform profile on the temperature profiles. For both waveform profiles, at the commencement of the oscillating cycle, a simultaneous decrease is observed for both wall and bulk temperatures. As a result of a gradual deceleration stage, a steady increase in the magnitudes of temperature profiles is observed throughout phases $\pi \leq \theta \leq 3\pi/2$ for the leading case. Whereas in the lagging case, due to the acute directional shift in the flowrate before the deceleration stage, the lowest oscillating wall and bulk temperatures are reached at phase π. During the acceleration stage between $\pi \leq \theta \leq 2\pi$, for the leading case, the oscillating wall and bulk temperature profiles do not evidently adjust to the directional change of the flowrate

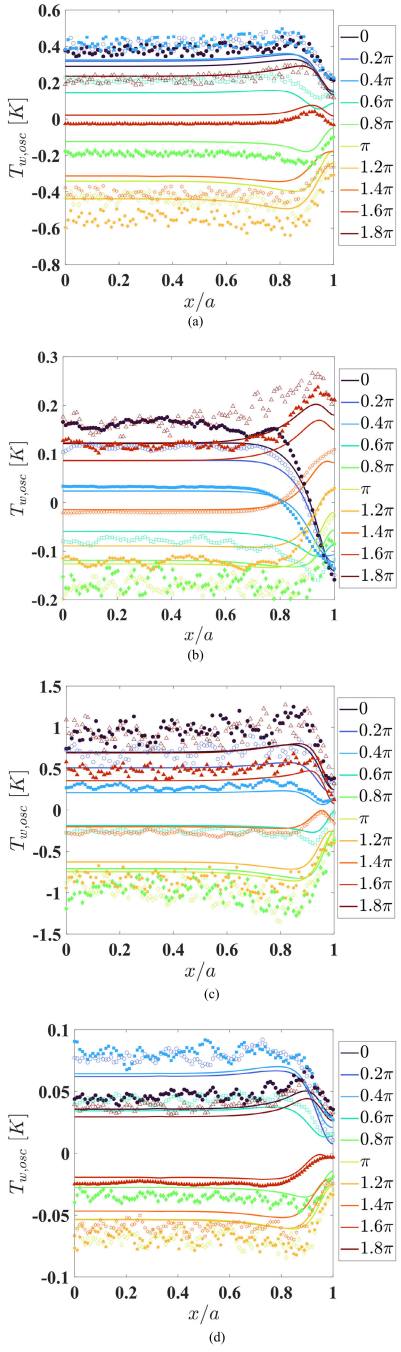

Fig. 7. Oscillating temperature profiles at the heated wall ($y/b = 0$) along the normalized spanwise direction (x/a). Solid lines represent CFD data, markers show the experimental data. (a) Leading asymmetric sinusoidal waveform, $f = 0.5$ Hz, $Wo = 2.5$, $A_0 = 0.5$. (b) Leading asymmetric sinusoidal waveform, $f = 0.5$ Hz, $Wo = 2.5$, $A_0 = 3$. (c) Lagging asymmetric sinusoidal waveform, $f = 0.5$ Hz, $Wo = 2.5$, $A_0 = 0.5$. (d) Lagging asymmetric sinusoidal waveform, $f = 0.5$ Hz, $Wo = 2.5$, $A_0 = 3$.

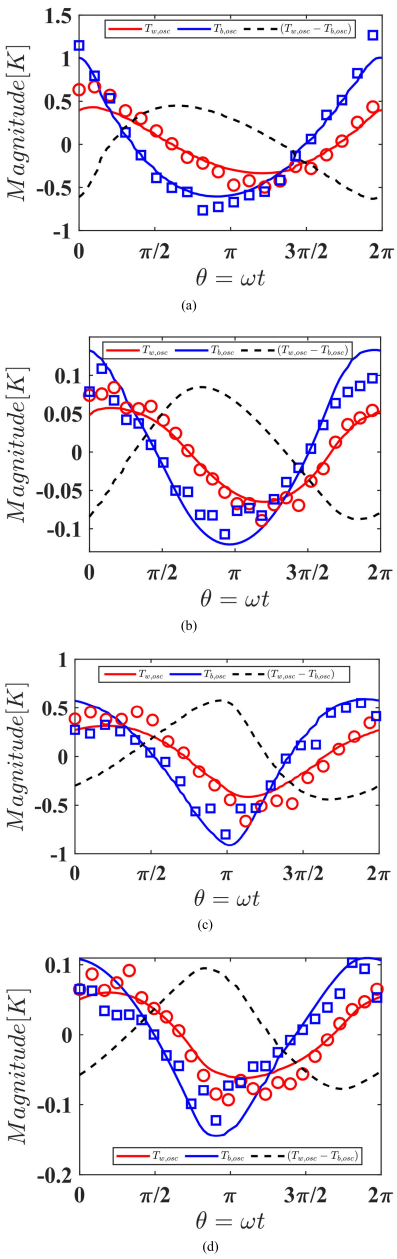

Fig. 8. Temporal variation of oscillating wall and bulk temperatures and the corresponding driving temperature difference. Solid lines represent CFD data, markers show the experimental data. (a) Leading asymmetric sinusoidal waveform, $f = 0.5$ Hz, $Wo = 2.5$, $A_0 = 0.5$. (b) Leading asymmetric sinusoidal waveform, $f = 0.5$ Hz, $Wo = 2.5$, $A_0 = 3$. (c) Lagging asymmetric sinusoidal waveform, $f = 0.5$ Hz, $Wo = 2.5$, $A_0 = 0.5$. (d) Lagging asymmetric sinusoidal waveform, $f = 0.5$ Hz, $Wo = 2.5$, $A_0 = 3$.

and thus settle with a steady increase of magnitudes. For the lagging case, the wall and bulk temperatures increase gradually to a maximum magnitude in accordance with the gradual acceleration toward the end of the cycle. With an increase in the flowrate amplitude, both waveform profiles exhibit a pronounced effect on the bulk temperatures suggesting enhanced removal of heat. As a result, the driving temperature difference shows a higher magnitude during the first half of the acceleration stage to symbolize effective heat withdrawal while the magnitudes settle in the deceleration cycle as it is comparatively weaker.

Fig. 9 plots the variation of the space-averaged instantaneous Nusselt number (|Nu|) for leading and lagging asymmetric pulsations at $Wo = 2.5$ and varying A_0. For the leading case, the |Nu| profiles react gradually to the asymmetric flowrate as described by Fig. 6(a) and (b). The peak magnitudes are shifted away from phase π. Similarly for the lagging case, as reflected from the flowrate profile in Fig. 6(c) and (d) an acute shift in deceleration is evident from the evolution of the |Nu| profile. A peak magnitude occurs

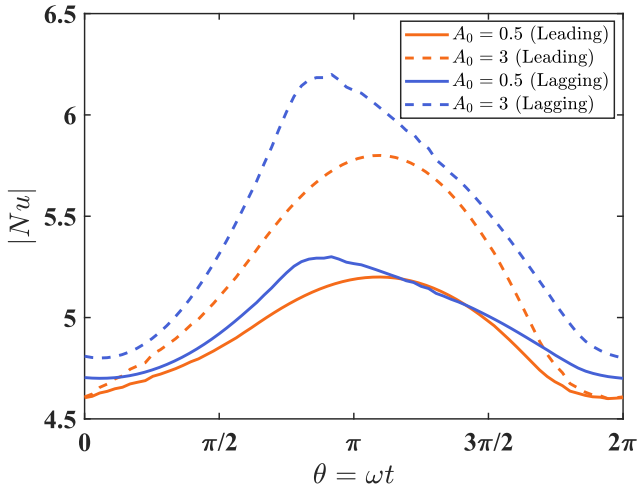

Fig. 9. Temporal variation of the space-averaged instantaneous Nusselt number (|Nu|) for leading and lagging asymmetric sinusoidal waveforms for $Wo = 2.5$ with varying A_0. For reference, the steady flow $Nu_s = 5.08$.

just before phase π. Across both the asymmetric formats, the highest flowrate amplitude of $A_0 = 3$ produces a maximum effect on the |Nu| profile. This is because of an increased influx of colder fluid from the stronger oscillating flow component over the underlying steady flow component. An increase in heat transfer is demonstrated since the convection term of the energy equation becomes more pronounced at higher flowrate amplitudes. The difference in Nusselt number for leading and lagging asymmetric profile as calculated from (7) results in a moderate enhancement of 4.2%, while the lagging asymmetric profile generates up to 11.1% enhancement over the corresponding steady flow for the case of $Wo = 2.5$, $A_0 = 3$.

Table I shows the calculated value of the thermal-hydraulic performance parameter (η) for each of the pulsating flow cases presented in this study. For a flow rate amplitude of $A_0 = 0.5$, the underlying steady component is stronger than the oscillating component, and thus, has a greater influence during the pulsation. A deterioration in thermal-hydraulic performance is observed for both leading and lagging asymmetric sinusoidal pulsation waveforms at $A_0 = 0.5$. However, for a higher flow rate amplitude of $A_0 = 3$, where the oscillating component has a greater influence than the underlying steady flow, increases in thermal-hydraulic are noted with a peak of $\eta = 2.5$ for the lagging asymmetric sinusoidal pulsation waveform. Thus, it can be concluded that irrespective of the presence of greater frictional losses, the thermal-hydraulic characteristics offered by asymmetric flows can result in improved overall performance compared to an equivalent steady flow under certain circumstances, which may be of benefit to applications involving pumped liquid cooling in confined spaces, such as CPU/GPU cooling.

V. Conclusion

Leading and lagging asymmetric sinusoidal single-phase laminar pulsating flows of $Wo = 2.5$ at flow rate amplitudes of $A_0 = 0.5, 3$ are numerically and experimentally investigated to evaluate the heat transfer potential. As per the authors' knowledge, this forms the first spatial and temporal heat transfer analysis for flow pulsations in a minichannel imposed with asymmetric sinusoidal waveforms. An IRT technique is implemented to examine the transverse wall temperatures

TABLE I
Thermal-Hydraulic Performance Data at Varying Flow Rate Amplitudes for Leading and Lagging Asymmetric Waveform Cases

Asymmetric sinusoidal waveform	Pulsation flow rate amplitude, (A_0), at $Wo = 2.5$	Thermal-hydraulic performance (η)
Lagging	0.5	0.5
Lagging	3	2.5
Leading	0.5	0.4
Leading	3	1.3

of a rectangular minichannel with a bottom heated wall. A corresponding 3-D transient conjugate heat transfer model is developed with a volumetric heat generation. The leading asymmetric format is characterized by a rapid increase of flowrate and pressure gradient in the acceleration stage followed by a gradual deceleration before the onset of the acceleration stage with restart of the cycle. The lagging asymmetric format comprises an initial period of gradual acceleration followed by an acute shift to the deceleration stage before another acceleration as the cycle restarts. The increase of flowrate amplitude and strengthening of the oscillating component results in a simultaneous increase of pressure gradient and shear stress magnitudes. An evolution of phase lag appears between the flowrate and pressure gradient profiles. The intensification of fluid momentum due to high oscillating flowrate amplitudes causes enhanced mixing in the near-wall and bulk regions of the channel, shown by the wall temperature profiles for lagging and leading cases, respectively. The presence of wall viscous forces leads to the phenomenon of annular effects which has been widely investigated in the literature for spanwise velocity and temperature cases of symmetric flow profiles. The wall and bulk temperature profiles tend to readily adjust to this rapidly fluctuating flow. Low flowrate amplitude flows present increased diffusion of heat from the heated wall to the bulk core region. Whereas with an increase in the flowrate amplitude, the wall and bulk temperatures are reduced. The effect of high pulsation flow rate amplitude leads to a heat transfer enhancement of about 11% over steady flow due to increased forced convection effects in the streamwise direction. When considering both heat transfer and hydraulic performance, the lagging asymmetric sinusoidal pulsation was found to offer a more notable improvement (2.5×) over steady flow which is of relevance to low electric power liquid pumping applications in small AR channels, such as those used in microprocessor cooling.

Acknowledgment

The authors thank the School of Engineering for the funding support. Additionally, they are grateful for the high-performance computing support from Trinity Center for High Performance Computing (TC-HPC) and Irish Center for High-End Computing (ICHEC).

References

[1] S. Sirikasemsuk, S. Wiriyasart, R. Prurapark, N. Naphon, and P. Naphon, "Water/nanofluid pulsating flow in thermoelectric module for cooling electric vehicle battery systems," *Int. J. Heat Technol.*, vol. 39, no. 5, pp. 1618–1626, Oct. 2021, doi: 10.18280/IJHT.390525.

[2] H. P. de Bock, P. Chamarthy, J. L. Jackson, and B. Whalen, "Investigation and application of an advanced dual piezoelectric cooling jet to a typical electronics cooling configuration," in *Proc. 13th InterSoc. Conf. Thermal Thermomech. Phenomena Electron. Syst.*, 2012, pp. 1387–1394, doi: 10.1109/ITHERM.2012.6231582.

[3] T. Fukue, H. Shirakawa, and W. Hiratsuka, "Basic study on flow and heat transfer control around heating components in rectangular duct by pulsating flow," in *Proc. 15th Int. Conf. Fluid Control, Meas. Vis.*, May 2019, pp. 1–6.

[4] M. Kichima, T. Fukue, and K. Hirose, "Basic study on flow and heat transfer performance of pulsating air flow for application to electronics cooling," in *Proc. Int. Conf. Electron. Packag. (ICEP)*, Apr. 2014, pp. 64–68, doi: 10.1109/ICEP.2014.6826662.

[5] H. Zhang, S. Li, J. Cheng, Z. Zheng, X. Li, and F. Li, "Numerical study on the pulsating effect on heat transfer performance of pseudo-plastic fluid flow in a manifold microchannel heat sink," *Appl. Thermal Eng.*, vol. 129, pp. 1092–1105, Jan. 2018, doi: 10.1016/j.applthermaleng.2017.10.124.

[6] J. R. Womersley, "Method for the calculation of velocity, rate of flow and viscous drag in arteries when the pressure gradient is known," *J. Physiol.*, vol. 127, no. 3, pp. 553–563, Mar. 1955, doi: 10.1113/jphysiol.1955.sp005276.

[7] B. Mehta and S. Khandekar, "Local experimental heat transfer of single-phase pulsating laminar flow in a square mini-channel," *Int. J. Thermal Sci.*, vol. 91, pp. 157–166, May 2015, doi: 10.1016/j.ijthermalsci.2015.01.008.

[8] T. E. Walsh, K. T. Yang, V. W. Nee, and Q. D. Liao, "Forced convection cooling in microelectronic cabinets via oscillatory flow techniques," in *Experimental Heat Transfer, Fluid Mechanics and Thermodynamics 1993*. 2013, pp. 641–648, doi: 10.1016/B978-0-444-81619-1.50076-9.

[9] R. Wälchli et al., "Radially oscillating flow hybrid cooling system for low profile electronics applications," in *Proc. 24th Annu. IEEE Semiconductor Thermal Meas. Manage. Symp.*, Mar. 2008, pp. 142–148, doi: 10.1109/STHERM.2008.4509381.

[10] R. Wälchli, T. Brunschwiler, B. Michel, and D. Poulikakos, "Self-contained, oscillating flow liquid cooling system for thin form factor high performance electronics," *J. Heat Transf.*, vol. 132, no. 5, May 2010, Art. no. 051401, doi: 10.1115/1.4000456.

[11] R. Blythman, T. Persoons, N. Jeffers, and D. B. Murray, "Heat transfer of laminar pulsating flow in a rectangular channel," *Int. J. Heat Mass Transf.*, vol. 128, pp. 279–289, Jan. 2019, doi: 10.1016/j.ijheatmasstransfer.2018.08.109.

[12] C. Xu, S. Xu, Z. Wang, and D. Feng, "Experimental investigation of flow and heat transfer characteristics of pulsating flows driven by wave signals in a microchannel heat sink," *Int. Commun. Heat Mass Transf.*, vol. 125, Jun. 2021, Art. no. 105343, doi: 10.1016/j.icheatmasstransfer.2021.105343.

[13] J. McEvoy, S. Alimohammadi, and T. Persoons, "Experimental investigation of flow pulsation waveforms in rectangular mesochannels for high heat flux electronics cooling," *Exp. Thermal Fluid Sci.*, vol. 109, Dec. 2019, Art. no. 109885, doi: 10.1016/j.expthermflusci.2019.109885.

[14] R. Blythman, T. Persoons, N. Jeffers, K. P. Nolan, and D. B. Murray, "Localised dynamics of laminar pulsatile flow in a rectangular channel," *Int. J. Heat Fluid Flow*, vol. 66, pp. 8–17, Aug. 2017, doi: 10.1016/j.ijheatfluidflow.2017.05.006.

[15] P. S. Kumavat, S. Alimohammadi, and S. M. O'Shaughnessy, "Heat transfer enhancement in a minichannel due to asymmetric sinusoidal pulsating flows," in *Proc. 28th Int. Workshop Thermal Invest. ICs Syst. (THERMINIC)*, Sep. 2022, pp. 1–6, doi: 10.1109/THERMINIC57263.2022.9950645.

[16] R. Siegel and J. M. Savino, "An analytical solution of the effect of peripheral wall conduction on laminar forced convection in rectangular channels," *J. Heat Transf.*, vol. 87, no. 1, pp. 59–66, Feb. 1965.

[17] R. K. Shah and A. L. London, "Thermal boundary conditions and some solutions for laminar duct flow forced convection," *J. Heat Transf.*, vol. 96, no. 2, pp. 159–165, May 1974.

[18] M. Spiga and G. L. Morini, "Nusselt numbers in laminar flow for H2 boundary conditions," *Int. J. Heat Mass Transf.*, vol. 39, no. 6, pp. 1165–1174, 1996, doi: 10.1016/0017-9310(95)00205-7.

[19] P. S. Kumavat, S. Alimohammadi, and S. M. O'Shaughnessy, "A computational conjugate heat transfer study of a rectangular minichannel undergoing sinusoidal flow pulsations," *Int. J. Thermal Sci.*, vol. 182, Dec. 2022, Art. no. 107790, doi: 10.1016/j.ijthermalsci.2022.107790.

[20] F. Durst, S. Ray, B. Ünsal, and O. A. Bayoumi, "The development lengths of laminar pipe and channel flows," *J. Fluids Eng.*, vol. 127, no. 6, pp. 1154–1160, Nov. 2005, doi: 10.1115/1.2063088.

[21] S. Ray, B. Ünsal, and F. Durst, "Development length of sinusoidally pulsating laminar pipe flows in moderate and high Reynolds number regimes," *Int. J. Heat Fluid Flow*, vol. 37, pp. 167–176, Oct. 2012, doi: 10.1016/j.ijheatfluidflow.2012.06.001.

[22] M. Abramowitz and I. Stegun, *Handbook of Mathematical Functions With Formulas, Graphs, and Mathematical Tables*. 1972.

[23] A. Bejan, *Convection Heat Transfer*. Hoboken, NJ, USA: Wiley, 2013.

[24] M. Ochs, T. Horbach, A. Schulz, R. Koch, and H.-J. Bauer, "A novel calibration method for an infrared thermography system applied to heat transfer experiments," *Meas. Sci. Technol.*, vol. 20, no. 7, Jul. 2009, Art. no. 075103, doi: 10.1088/0957-0233/20/7/075103.

[25] P. Kumavat and S. M. O'Shaughnessy, "Experimental investigation of heat transfer enhancement by pulsating flow in a minichannel," *J. Phys., Conf. Ser.*, vol. 2116, no. 1, Nov. 2021, Art. no. 012031, doi: 10.1088/1742-6596/2116/1/012031.

Parth S. Kumavat received the Ph.D. degree in mechanical engineering with the Trinity College, University of Dublin, Dublin, Ireland.

His Ph.D. research was focused on active heat transfer enhancement in liquid cooling systems using combined numerical and experimental methods and is subjected to the conferral of degree in the summer of 2023. He has 5 years of experience as a Teaching Assistant and a Laboratory Demonstrator delivering heat transfer and fluid dynamics modules. In the recent past, he has worked and delivered several computational modeling projects on heat sinks and cryocooling as a research associate at international institutions notably RWTH Aachen, Aachen, Germany, in 2016, and Indian Institute of Technology, Bombay, India, in 2017. Since 2023, he has been working as a Research Assistant on an industry-funded project with the Department of Mechanical Engineering, Trinity College, University of Dublin. His current area of work is involved with phase change behavior on nanoscale functional surfaces for thermosiphon applications.

Sajad Alimohammadi received the Ph.D. degree from Trinity College Dublin (TCD), Dublin, Ireland, in 2015.

He is a Lecturer of mechanical engineering at TU Dublin, Ireland. He also serves as an Adjunct Assistant Professor, Trinity College Dublin, in 2018. He worked as a Research Assistant at TU Brunswick, Brunswick, Germany, in 2011. In 2015, he served as a Post-Doctoral Research Fellow at TCD and an Adjunct Research Staff Member at the Cooling Technologies Research Center, Purdue University, West Lafayette, IN, USA. His teaching and research interests are focused on applied thermofluids sciences and novel energy efficiency technologies using experimental and numerical methods.

Séamus M. O'Shaughnessy is an Ussher Assistant Professor with the Energy and Sustainable International Development, Department of Mechanical, Manufacturing, and Biomedical Engineering, Trinity College, University of Dublin, Dublin, Ireland. For almost 20 years, he has specialized in the research fields of fluid mechanics and heat transfer. He supervises a diverse group of researchers, and his research interests include both fundamental and applied investigations using analytical, computational, and experimental techniques. His core teaching include thermodynamics, fluid mechanics, and computational fluid dynamics.